



# Tunable Single-Photon Scattering of a Giant $\Lambda$ -type Atom in a SQUID-Chain Waveguide

Jian-Ping Zou, Rui-Yang Gong and Ze-Liang Xiang\*

School of Physics, Sun Yat-Sen University, Guangzhou, China

We study single-photon scattering of an artificial giant  $\Lambda$ -type atom coupled to a superconducting quantum interference device (SQUID) chains waveguide at two points. In this circuit, the single-photon scattering rates are dependent on the atom-waveguide coupling strengths and the phase accumulated between two coupling points. By modulating the flux-dependent phase velocity in the SQUID-chain waveguide, the photon's traveling time is changed, and the accumulating phase is adjusted simultaneously. We investigate the relationship between the scattering effect and the flux bias, which allows us to explore novel phenomena with the tunable traveling time in both Markovian and non-Markovian regimes, and to design novel quantum technologies such as quantum storage.

## OPEN ACCESS

### Edited by:

Zhihai Wang,  
Northeast Normal University, China

### Reviewed by:

Re-Bing Wu,  
Tsinghua University, China  
Chang-Sheng Hu,  
Huazhong University of Science and  
Technology, China

### \*Correspondence:

Ze-Liang Xiang  
xiangzliang@mail.sysu.edu.cn

### Specialty section:

This article was submitted to  
Quantum Engineering and  
Technology,  
a section of the journal  
Frontiers in Physics

Received: 15 March 2022

Accepted: 07 April 2022

Published: 27 April 2022

### Citation:

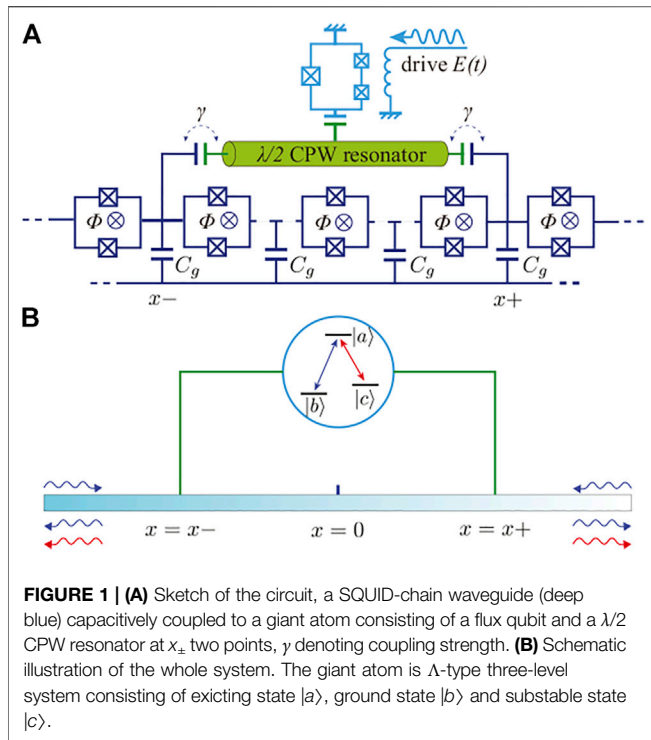
Zou J-P, Gong R-Y and Xiang Z-L  
(2022) Tunable Single-Photon  
Scattering of a Giant  $\Lambda$ -type Atom in a  
SQUID-Chain Waveguide.  
Front. Phys. 10:896827.  
doi: 10.3389/fphy.2022.896827

**Keywords:** quantum optics, waveguide QED, superconducting circuit, giant atom, non-markovian dynamics

## 1 INTRODUCTION

In the last decades, research on superconducting quantum circuits has gone far forwards [1,2]. The superconducting quantum circuit is blessed with scalability, integrability, and flexibility interacting with other systems, making it a prospective platform for carrying on the quantum information and quantum computation missions [3-5]. The superconducting qubit can play a role as an artificial atom and then strongly coupled to microwave photons in circuit quantum electrodynamics (cQED) [6-17]. One can make the artificial atom's scale comparable to wavelengths so that it goes beyond the dipole approximation [18]. Moreover, the artificial atoms can also couple with the field confined in a waveguide at several points, which behave as a giant atom [18]. In recent years, a giant atom system has been experimentally realized for the first time in an acoustic system, where a superconducting qubit coupled to a surface acoustic wave (SAW) via an interdigital transducer acts as a giant atom [19,20], the photonic version following [21,22]. In such giant atom systems, many striking effects were discovered [18]. For example, strongly frequency-dependent coupling between giant atoms and bosonic modes can be designed for realizing interference effects [23-26] between coupling points, which enables electromagnetically induced transparency (EIT) in a ladder configuration [27]. When the distance of the coupling points is too large, the Markovian approximation can no longer be applied to the whole system. The so-called non-Markovian effect [28] induced by the non-negligible travel time can cause some novel phenomena in giant-atom systems [29], such as non-exponential decay [30] and bound state in a continuum [31,32].

Waveguide quantum electrodynamics (wQED) [33] studies the interaction between an atom and continuum of electromagnetic modes confined in a 1D waveguide. WQED uses the transmission and reflection spectrum of the incident field to reveal the dynamics of the whole system and supports a theoretical basis for quantum networks. Because of recent



experimental advances on giant atoms [19,20], wQED setups based on giant atoms have attracted considerable attention. For example, Ref. [34] proposed a decoherence-free waveguide with multiple giant atoms. In addition, an effective single-photon frequency conversion rate via a giant  $\Lambda$ -type atom can approach a unit combining with the Sagnac interferometer [35]. Compared to the two-level atom, the  $\Lambda$ -type three-level atom has two transition paths, which provide additional tunable spaces. Meanwhile, the circuit  $\Lambda$ -type atom has been demonstrated good tunability in experiments, as shown in Refs [36,37]. The combination of  $\Lambda$ -type atoms and giant atoms could be a promising way for quantum information processing, which will be explored in this paper. Very recently, Ref. [32] proposed tunable chiral bound states in a system composed of superconducting giant atoms and a Josephson photonic-crystal waveguide [38-42].

In this paper, we present a circuit giant  $\Lambda$ -type atom couples to the SQUID-chain waveguide. In contrast to previous works with a fixed length between two coupling points, we replace a typical SQUID-chain waveguide instead of a standard transmission line and achieve the in-situ tunability of traveling time. This tunability stems from the flux-dependent phase velocity of the SQUID-chain waveguide. By studying single-photon scattering in this system, we can understand the unique dynamics of the giant atom. Then, the tunable group velocity of this particular waveguide can be utilized to realize the tunable scattering rate. Furthermore, taking advantage of the tunability of this circuit, we explore the novel physical phenomena from Markovian to non-Markovian regimes and propose a promising protocol to store quantum information.

The paper is structured as follows. We begin in **Section 2** with a brief introduction of the Hamiltonian of the whole system before turning to the detailed calculation of the single-photon process in the SQUID-chain waveguide in **Section 3**. Then, distinguishing scattering properties of this system from Markovian to Non-Markovian regimes and an application in quantum storage are discussed in **Section 4**. At last, we end with a conclusion in **Section 5**.

## 2 MODEL

We consider a giant  $\Lambda$ -type atom interacting with a 1D waveguide at two coupling points, as depicted in **Figure 1**. The Hamiltonian  $H$  is defined as

$$H = H_a + H_w + H_{\text{int}}, \quad (1)$$

where  $H_a = \hbar \sum_{i=a,b,c} \omega_i |i\rangle \langle i|$  is the free Hamiltonian of the  $\Lambda$ -type atom, where  $|a\rangle$ ,  $|b\rangle$  and  $|c\rangle$  are the ground, excited and substable states, respectively. Such a  $\Lambda$ -type atom can be experimentally implemented in a circuit QED system, where a flux qubit couples to a coplanar waveguide (CPW) resonator with a resonant driving field [36,37].

$H_w$  describes a bidirectional waveguide where photons propagate equally in two directions. In our setup, the waveguide is a superconducting transmission line composed of identical SQUID loops. The interval between adjacent loops equals  $d_0$ , and a homogeneous magnetic field is applied vertically through every SQUID loop. The SQUID loop can be viewed as an effective inductance  $L_j$  parallel to the Josephson capacitance  $C_j$ . The Hamiltonian of SQUID chains can be quantized as [39]:  $H_{sc} = \sum_k \omega_k (a_k^\dagger a_k + 1/2)$ , where  $a_k$  ( $a_k^\dagger$ ) is the annihilation (creation) operator of mode  $k$ . And the SQUID-chain waveguide has a dispersion relation form [32]:

$$\omega_k = \frac{1}{\sqrt{L_j C_j}} \sqrt{\frac{1 - \cos(kd_0)}{C_j / C_g [1 - \cos(kd_0)] + \frac{1}{2}}}. \quad (2)$$

For the effective inductance of SQUID,  $L_j$  is flux dependent, the photon's group velocity  $v_g = d\omega/dk$  in the waveguide is, therefore, a tunable parameter. Assuming the waveguide length  $L \rightarrow \infty$ , we obtain the continuum form of the Hamiltonian

$$H_w = \int \hbar \omega_k a_k^\dagger a_k d\omega_k. \quad (3)$$

$H_{\text{int}}$  represents the coupling of two circuit systems and has the form,  $H_{\text{int}} \propto \sqrt{\tilde{\kappa}_{ij}^\pm} / 2\pi (\tilde{\sigma}_{ij} a_k e^{ikx_\pm} + a_k^\dagger \tilde{\sigma}_{ji} e^{-ikx_\pm})$ , where  $\tilde{\sigma}_{ij} = |i\rangle \langle j|$  is the transition operator of atom, and  $\tilde{\kappa}_{ij}^\pm = \kappa |\langle i|a^\dagger|j\rangle|^2$  denote the coupling strengths between the circuit  $\Lambda$ -type atom and the SQUID-chain waveguide, with  $\kappa$  being the decay rate of the resonator through two gate capacitances  $C_g^\pm$  at two points  $x_\pm$  (details in Appendix A).

Although the whole system may reach the non-Markovian regime originating from two distant coupling points, the Markovian approximation is still valid at each local coupling point  $x_\pm$ . Consequently, the total Hamiltonian for the whole system can be written as

$$\begin{aligned}
H = & \hbar \sum_{i=a,b,c} \omega_i |i\rangle \langle i| + \sum_{\alpha=1,2} \int \hbar \omega_p a_{\alpha\omega_p}^\dagger a_{\alpha\omega_p} d\omega_p \\
& + \sum_{\alpha=1,2} \int \hbar \sqrt{\frac{\gamma_1}{4\pi}} [ |b\rangle \langle a| a_{\alpha\omega_k}^\dagger (e^{-i\omega_k k_x L/2} + e^{i\omega_k k_x L/2}) \\
& + \text{H.c.}] d\omega_k + \sum_{\alpha=1,2} \int \hbar \sqrt{\frac{\gamma_2}{4\pi}} [ |c\rangle \langle a| a_{\alpha\omega_q}^\dagger (e^{-i\omega_q k_x L/2} \\
& + e^{i\omega_q k_x L/2}) + \text{H.c.}] d\omega_q.
\end{aligned} \quad (4)$$

The terms on the right-hand side of the first line are the atom and field modes free energy, where  $|i\rangle$  and  $\omega_i$  are the eigenstates of the atomic system and their energies, respectively.  $a_{\alpha\omega_p}$  are photon field operators for the right ( $\alpha = 1$ ) and left-propagating ( $\alpha = 2$ ) photons, satisfying  $[a_{\alpha\omega_p}, a_{\alpha'\omega_p}^\dagger] = \delta_{\alpha\alpha'} \delta(\omega_p - \omega_p')$ , where  $\omega_p$  represent the frequency of the mode.  $k_p$  is the wave vector corresponding to  $\omega_p$ , satisfying  $\omega_p = k_p v_g$ . The coupling terms in the last three lines have involved the phase difference between two coupling points at positions  $x_{\pm} = \pm L/2$ .  $\gamma_i$  denote the radiative decay rates for two transition paths of the  $\Lambda$ -type level configuration, and they also represent the coupling strength, which is approximated as constants here over the relevant frequency range in the spirit of Weisskopf-Wigner theory.

### 3 SINGLE-PHOTON PROCESS IN SQUID-CHAIN WAVEGUIDES

#### 3.1 Dynamics of the Giant Atom

Firstly, the motion equations of the giant atom limited in the single-photon subspace can be studied by using the similar method introduced in Ref [29]. The total state of a  $\Lambda$ -type giant atom and the microwave field in the waveguide can be described by

$$\begin{aligned}
|\Phi(t)\rangle = & C_a(t) |a, 0\rangle + \sum_{\alpha=1,2} \int d\omega_k C_{b\alpha k}(t) |b, 1_k\rangle \\
& + \sum_{\alpha=1,2} \int d\omega_q C_{c\alpha q}(t) |c, 1_q\rangle,
\end{aligned} \quad (5)$$

where  $|0\rangle$  represents the vacuum state of the microwave filed in the SQUID-chain waveguide. The integral terms describe the state of a single photon propagating in the waveguide towards right  $\alpha = 1$  or left  $\alpha = 2$ , with the giant atom in the ground state  $|b\rangle$  (or substable state  $|c\rangle$ ). Using the Schrödinger equation  $i\hbar \partial/\partial t |\Phi(t)\rangle = H|\Phi(t)\rangle$ , we obtain the differential equations for coefficients:  $C_a(t)$  being the probability amplitude of the giant atom in excited state  $|a\rangle$ ,  $C_{b1(2)k}$  and  $C_{c1(2)q}$  denoting the photon spectrums in the transmission line with the giant atom staying in the ground state  $|b\rangle$  and the substable state  $|c\rangle$ , respectively. The time evolution of  $C_a(t)$  is then turned to

$$\begin{aligned}
\frac{dC_a(t)}{dt} = & -i\omega_a C_a(t) - \gamma_1 [C_a(t) \\
& + \Theta(t-T) e^{-i\omega_b T} C_a(t-T)] - \gamma_2 [C_a(t) + \Theta(t-T) e^{-i\omega_c T} C_a(t-T)] \\
& - i\sqrt{\frac{\gamma_1 v_g}{2}} e^{-i\omega_b t} [C_{b1}(-L/2 - v_g t, 0) + C_{b1}(L/2 - v_g t, 0)] \\
& - i\sqrt{\frac{\gamma_1 v_g}{2}} e^{-i\omega_b t} [C_{b2}(-L/2 + v_g t, 0) + C_{b2}(L/2 + v_g t, 0)] \\
& - i\sqrt{\frac{\gamma_2 v_g}{2}} e^{-i\omega_c t} [C_{c1}(-L/2 - v_g t, 0) + C_{c1}(L/2 - v_g t, 0)] \\
& - i\sqrt{\frac{\gamma_2 v_g}{2}} e^{-i\omega_c t} [C_{c2}(-L/2 + v_g t, 0) + C_{c2}(L/2 + v_g t, 0)].
\end{aligned} \quad (6)$$

The first term denotes free evolution. The following two terms show the atom relaxing process with  $\gamma_{1,2}$  and feedback effect with  $C_a(t-T)$ , where  $T = L/v_g$  is the delay time. Here,  $\Theta(\bullet)$  is the Heaviside step function showing the time-delay feedback between the coupling points. We introduced the notion  $C_{b1(2)}(x, t) = \frac{1}{\sqrt{2\pi v_g}} \int d\omega_k e^{i\omega_k x/v_g} C_{b1(2)k}(t)$  for describing photon distribution and time evolution. Then, the remaining four terms imply that the incident photon in both directions can excite the giant atom.

$C_a(t)$  can be analytically solved and finally has the spectrum form expansion (details in Appendix A)

$$\begin{aligned}
C_a(t) = & \frac{1}{2\pi i} \int_{\epsilon-i\infty}^{\epsilon+i\infty} C_a(s) e^{st} ds \\
= & \frac{1}{2\pi i} \int ds \frac{C_a(0) e^{st}}{s + i\omega_a + \gamma_1 D_1 + \gamma_2 D_2} \\
& - i\sqrt{\frac{\gamma_1}{4\pi}} \int ds \frac{C_{bs}(0) (e^{sT/2} + e^{-sT/2}) e^{st} e^{-i\omega_b t}}{s + i\omega_a + \gamma_1 D_1 + \gamma_2 D_2} \\
& - i\sqrt{\frac{\gamma_2}{4\pi}} \int ds \frac{C_{cs}(0) (e^{sT/2} + e^{-sT/2}) e^{st} e^{-i\omega_c t}}{s + i\omega_a + \gamma_1 D_1 + \gamma_2 D_2},
\end{aligned} \quad (7)$$

where  $D_{1(2)} = 1 + e^{-i\omega_{b(c)T}} e^{-sT}$  is the additional phase of the decay rate  $\gamma_{1(2)}$  due to the time-delay feedback effect. Here, we introduce the notations  $C_{bs}(0) = C_{b1s}(0) + C_{b2s}(0)$  and  $C_{cs}(0) = C_{c1s}(0) + C_{c2s}(0)$ , denoting the initial photon of frequency  $\omega_s$  in the waveguide incident from both direction.

#### 3.2 Single-Photon Scattering

To study scattering properties of the giant atom, we set a right-propagating photon incident into the waveguide, whose frequency is centered at  $\omega_k$  ( $C_{b1k} \neq 0$ ), with the giant atom initially being in the ground state. The dynamical evolution equation of the giant atom is then derived from Eq. 7,

$$C_a(t) = -i\sqrt{\frac{\gamma_1}{4\pi}} \int ds \frac{C_{b1s}(0) (e^{sT/2} + e^{-sT/2}) e^{st} e^{-i\omega_b t}}{s + i\omega_a + \gamma_1 D_1 + \gamma_2 D_2}. \quad (8)$$

In the long-time limit, the emission spectrum of outgoing photons can be obtained (details in Appendix B):

$$C_{b1k}(\infty) = e^{-i\omega_k t} C_{b1k}(0) \left[ 1 - \frac{\gamma_1 [1 + \cos(\omega_k T)]}{i(\omega_a - \omega_k) + \gamma_1 (1 + e^{i\omega_k T}) + \gamma_2 (1 + e^{i\omega_k T})} \right], \quad (9)$$

$$C_{b2k}(\infty) = e^{-i\omega_k t} C_{b1k}(0) \frac{-\gamma_1 [1 + \cos(\omega_k T)]}{i(\omega_a - \omega_k) + \gamma_1 (1 + e^{i\omega_k T}) + \gamma_2 (1 + e^{i\omega_k T})}, \quad (10)$$

$$C_{c1q}(\infty) = e^{-i\omega_k t} C_{b1k}(0) \frac{-2\sqrt{\gamma_1 \gamma_2} \cos(\omega_q T/2) \cos(\omega_k T/2)}{i(\omega_a - \omega_k) + \gamma_1 (1 + e^{i\omega_k T}) + \gamma_2 (1 + e^{i\omega_k T})}, \quad (11)$$

where the ground state energy is set to zero  $\omega_b = 0$  with variable substitution  $\omega_k = \omega_q + \omega_c$ . Then, we obtain the transmission rate  $T_k$ , the reflection rate  $R_k$ , and the forward conversion rate  $T_q$ ,

$$T_k = \left| \frac{C_{b1k}(\infty)}{C_{b1k}(0)} \right|^2 = \frac{(\omega_k - \omega_a - \gamma_1 \sin(\omega_k T) - \gamma_2 \sin(\omega_q T))^2 + \gamma_2^2 (1 + \cos(\omega_q T))^2}{(\omega_k - \omega_a - \gamma_1 \sin(\omega_k T) - \gamma_2 \sin(\omega_q T))^2 + [\gamma_1 (1 + \cos(\omega_k T)) + \gamma_2 (1 + \cos(\omega_q T))]^2}, \quad (12)$$

$$R_k = \left| \frac{C_{b2k}(\infty)}{C_{b1k}(0)} \right|^2 = \frac{\gamma_1^2 (1 + \cos(\omega_k T))^2}{(\omega_k - \omega_a - \gamma_1 \sin(\omega_k T) - \gamma_2 \sin(\omega_q T))^2 + [\gamma_1 (1 + \cos(\omega_k T)) + \gamma_2 (1 + \cos(\omega_q T))]^2}, \quad (13)$$

$$T_q = \left| \frac{C_{c1q}(\infty)}{C_{b1k}(0)} \right|^2 = \frac{4\gamma_1 \gamma_2 \cos^2(\omega_k T/2) \cos^2(\omega_q T/2)}{(\omega_k - \omega_a - \gamma_1 \sin(\omega_k T) - \gamma_2 \sin(\omega_q T))^2 + [\gamma_1 (1 + \cos(\omega_k T)) + \gamma_2 (1 + \cos(\omega_q T))]^2}. \quad (14)$$

In contrast to small atoms, **Eqs 12–14** imply that the giant atom has the corrected transition frequency  $\Omega_a = \omega_a + \gamma_1 \sin(\omega_k T) + \gamma_2 \sin(\omega_q T)$  and decay rate  $\Gamma_{1(2)} = \gamma_{1(2)}(1 + \cos(\omega_{k(q)} T))$  [43]. From **Eq. 13**, the conditions for total reflection,  $R_k = 1$ , can be obtained directly

$$\begin{aligned} \omega_a - \omega_k + \gamma_1 \sin(\omega_k T) + \gamma_2 \sin(\omega_q T) &= 0, \\ \gamma_2 [1 + \cos(\omega_q T)] &= 0. \end{aligned} \quad (15)$$

There are two ways to make the second condition satisfied. One is  $\gamma_2 = 0$ , which means the transition path  $|a\rangle \rightarrow |c\rangle$  directly turned off. The other one is  $\omega_q T = 2(n + 1)\pi$ , which infers that the decay channel of  $|a\rangle \rightarrow |c\rangle$  is suppressed by the destructive interference between coupling points [35]. Either of these two cases can cause that the  $\Lambda$  configuration atom could be reduced to a simple two-level atom. However, the first solution is trivial and will not be considered in our case. Then the two conditions in **Eq. 15** can be rewritten as  $\omega_k - \omega_a = \gamma_1 \sin(\omega_c T)$  and  $\omega_q T = 2(n + 1)\pi$ . Here, we introduce the detuning,  $\Delta = \omega_k - \omega_a$ , of the incident photon from the  $|a\rangle - |b\rangle$  transition. The total reflection conditions are written as  $\Delta = \gamma_1 \sin(\omega_c T)$  and  $\Delta = \omega_c - \omega_a + 2(n + 1)\pi/T$ .

While the total transmission,  $T_k = 1$  and  $R_k = T_q = 0$ , happens in the case of  $\omega_k T = (2n + 1)\pi$ , no matter with  $\omega_c T$ . Because of the nondirectional decay process of the excited atom, the forward nonelastic scattering photon strength is equal to the backward one. Thus, it is reasonable to set the frequency conversion rate to be twice the forward conversion rate,  $T_c = 2T_q$ . The fundamental source affecting the conversion rate is the ratio of the decay rates, i.e.,  $\gamma_1/\gamma_2$ . For simplicity, we set  $\gamma_1/\gamma_2 = 1$  and use  $\gamma$  regardless of the subscript in the context.

In **Figure 2**, we plot the scattering rates as the function of the scaled detuning  $\Delta/\gamma$  and the scaled substable level frequency  $\omega_c/\gamma$ , for  $\omega_a T = 2000\pi$ , where  $\omega_a/\gamma = 10,000$  and  $T = 0.2\pi/\gamma$ . **Figure 2A,B** depict the reflection rates for the Markovian ( $\gamma T = 0.2\pi$ ) and non-Markovian ( $\gamma T = 3\pi$ ) regimes, respectively. Compared with **Figure 2A,B** shows two different features. First, there are additional small peaks at two sides of the primary maximum for the certain  $\omega_c$ . Second, the frequency band of the total reflection is broadened. The giant atom can provide a wide spectrum window for the strong reflection in the non-Markovian regime. **Figure 2C,D** represent the single-photon transmittance and the frequency conversion rate, respectively, of the giant atom in the Markovian regime.

### 3.3 Tunable Traveling Time T

Based on the above investigation, it is clear that the single-photon scattering effect of the  $\Lambda$ -type giant atom is intensely affected by the two crucial phases,  $\omega_k T$  and  $\omega_c T$ . These phases are dependent on the atom's energy level structure and the coupling points separation distance. Therefore, it is intuitive to control the spatial length between the coupling points for coherently tuning the phase. However, the spatial length is fixed once the circuit sample is fabricated. Here, we introduce the SQUID-chain transmission line, in which the photon's phase velocity is flux-dependent. Although the spatial distance of two points in the waveguide is determined, changes in the photon's phase velocity will change the cost time  $T$  for photons traveling between two fixed points, equivalent to the effective length and accumulated phase. Consequently, the effect will affect the dynamical evolution of this  $\Lambda$ -type giant atom as well as the scattering properties.

In addition to infinite length condition  $L \rightarrow \infty$ , if the superconducting transmission line also satisfies following conditions [32]:

$$d_0 \ll \lambda_k \ll L, k \ll \frac{1}{d_0} \sqrt{\frac{C_g}{C_J}}, \quad (16)$$

the dispersion relation **Eq. 2** can be reduced to

$$\omega_{k0} \approx \frac{kd_0}{\sqrt{L_J C_g}} = kv_J, \quad (17)$$

i.e., the phase velocity is  $d_0/\sqrt{L_J C_g}$ . The effective inductance of the SQUID is controlled by the magnetic field through it. Then the photon's phase velocity  $v$  can be modulated by controlling the field through the SQUID loops

$$v = \frac{d_0}{\sqrt{L_J C_g}} = \frac{d_0 \sqrt{\cos(\pi\Phi/\Phi_0)}}{\sqrt{L_0 C_g}}. \quad (18)$$

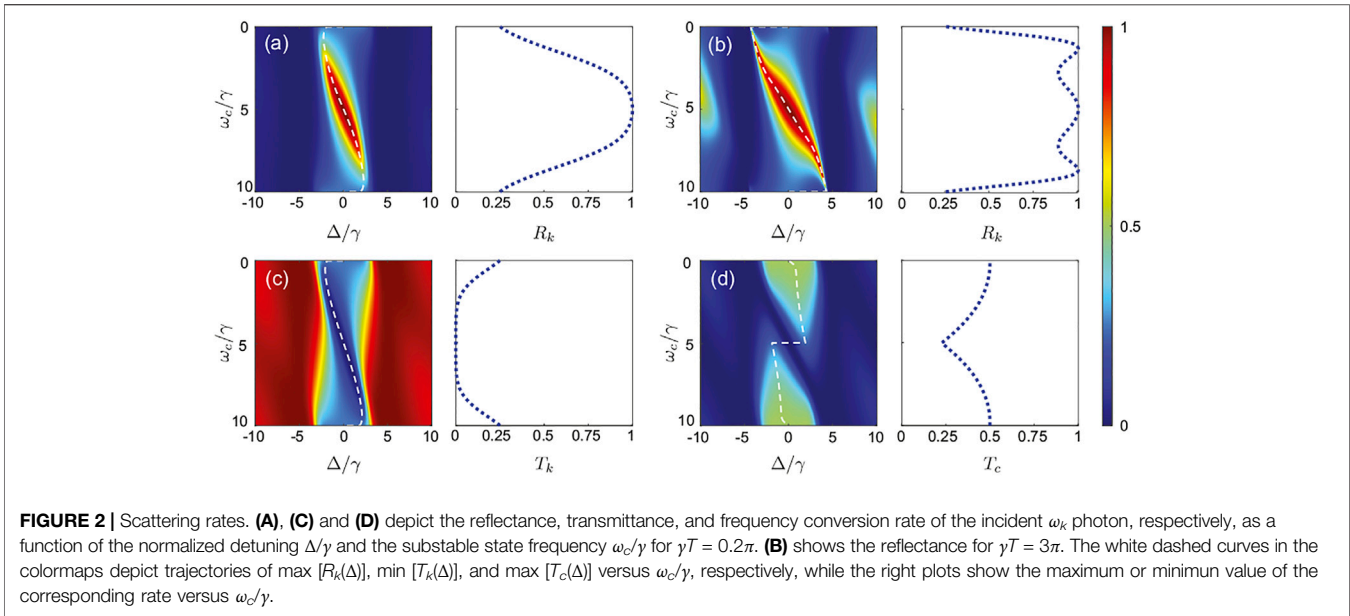
The change in phase velocity leads to the change of the traveling time of photons propagating between two points, so does the accumulating phase. We set the separation distance of the two coupling points as  $d = nd_0$ , i.e.,  $n$  SQUIDs constituting the waveguide between the coupling points. Then, the traveling time of a photon is

$$T = \frac{d}{v} = \frac{n\sqrt{L_0 C_g}}{\sqrt{\cos(\pi\Phi/\Phi_0)}}. \quad (19)$$

By modulating the photon's traveling time between two coupling points, we can explore some interesting applications that will be discussed in **Section 4**.

### 3.4 Experimental Feasibility

The linear dispersion relation (17) of the SQUID-chain waveguide is valid over a wide frequency domain  $\omega_k < 10$  GHz, when the circuit parameters are taken as [32]; [41,40]:  $L_0 = 0.2$  nH,  $C_g = 0.4$  fF,  $C_J = 90$  fF,  $d_0 = 1$   $\mu$ m. The transition frequencies of the circuit  $\Lambda$ -type atom can be set to fall within the frequency domain. For example, we can take these parameters:  $\omega_{ac}/2\pi = 6.4828$  GHz,  $\omega_{ab}/2\pi \approx 6.48452$  GHz under a



driving field with the frequency  $\omega_d/2\pi = 5.6466$  GHz and the coupling strength  $\Omega_d/2\pi = 1.46$  MHz [37], where  $\omega_{ab(c)} = \omega_a - \omega_{b(c)}$  is the transition frequency between  $|a\rangle$  and  $|b(c)\rangle$ . The original traveling time now is  $T_0 \approx 10^{-9}$  s without the magnetic field. With normal reliable decay rates  $\gamma$  ( $\sim$ MHz) for the capacitive coupling, we can realize  $\gamma T$  changing from the regime of  $\gamma T \ll 1$  to  $\gamma T \approx 1$  theoretically. In other words, the whole system can transit to the non-Markovian regime from the Markovian regime gradually. Thus, taking advantage of this setup, we can study novel physical phenomena in both Markovian and Non-Markovian regimes. It also allows fine-grained operations.

## 4 DISCUSSIONS

### 4.1 From Markovian to Non-markovian

For the sake of intuitively seeing the tunable scattering effects, we substitute Eq. 19 into Eq. 12–14 and obtain the relationship between the scattering rates and the flux bias as:

$$T_k = \frac{(\omega_k - \Omega_a)^2 + \Gamma_2^2}{(\omega_k - \Omega_a)^2 + (\Gamma_1 + \Gamma_2)^2}, \quad (20)$$

$$R_k = \frac{\Gamma_1^2}{(\omega_k - \Omega_a)^2 + (\Gamma_1 + \Gamma_2)^2}, \quad (21)$$

$$T_q = \frac{\Gamma_1 \Gamma_2}{(\omega_k - \Omega_a)^2 + (\Gamma_1 + \Gamma_2)^2}, \quad (22)$$

where the corrected transition frequency  $\Omega_a = \omega_a + \gamma_1 \sin\left(\frac{n\omega_k \sqrt{L_0 C_g}}{\sqrt{\cos(\pi\Phi/\Phi_0)}}\right) + \gamma_2 \sin\left(\frac{n\omega_g \sqrt{L_0 C_g}}{\sqrt{\cos(\pi\Phi/\Phi_0)}}\right)$  and decay rate  $\Gamma_{1(2)} = \gamma_{1(2)} [1 + \cos\left(\frac{n\omega_{k(q)} \sqrt{L_0 C_g}}{\sqrt{\cos(\pi\Phi/\Phi_0)}}\right)]$  are the functions of the flux bias. Then we plot the atom's scattering effect to characterize their relationship.

First, we demonstrate the giant atom's scattering characteristics  $R_k$ ,  $T_k$  and  $T_c$  as the function of the external scaled magnetic flux  $\Phi/\Phi_0$  and the scaled detuning from the excited state frequency  $\Delta/\gamma$  in **Figures 3A–C**. The decay rates and the energy level structure of the giant atom are set to  $\gamma_1 = \gamma_2 = \omega_c/10 = \omega_a/10000$ . The original traveling time of the photon is set as  $T_0 = 0.001/\gamma$ . **Figures 3A–C** clearly show that the scattering rate is a single value around zero flux. While the flux is increasing, the frequency band of the rates is broadened, as discussed in **Section 3.2**. Continue to increase magnetic flux approaching  $0.5\Phi_0$ , the scattering rates begin violently oscillating, which implies  $\gamma T > 1$  in the non-Markovian regime. Then, the detailed scattering rates of the system near the white dashed line in **Figures 3A–C** are shown in **Figures 3D–F**. The shape of scattering rates spreading out like a water wave demonstrates their periodicity, which originates from the cosine function of the magnetic flux. The flux  $\Phi_a$  along the white dashed line satisfies  $T_a = 1/\gamma = T_0/\sqrt{\cos(\pi\Phi_a/\Phi_0)}$ , while the blue dashed line corresponds to  $\Phi = 0$ . Therefore, the large region between the two white dashed lines is the parameter space of the Markovian regime, and the remaining edge areas are the parameter space of the non-Markovian regime. From the perspective of **Figure 3**, the adjustable ranges of the reflection rate and the transmission rate are 0,  $-1$ . The total reflection case only happens in the non-Markovian regime. The frequency conversion rate varies from 0,  $-0.5$  as the flux changes, which is limited by the ratio of the decay rates.

**Figures 4A–C** show the scattering rates  $R_k$ ,  $T_k$  and  $T_c$  along the cuts of dashed lines in **Figures 3A–C** versus the normalized detuning  $\Delta/\gamma$ . Here, the red curve describes the scattering rates for  $\gamma T = 1$  (the cut of white dashed lines), and the blue dashed curve describes the scattering rates for  $\gamma T = 0.001$  (the cut of blue dashed lines). The reflection rate and the transmission rate are

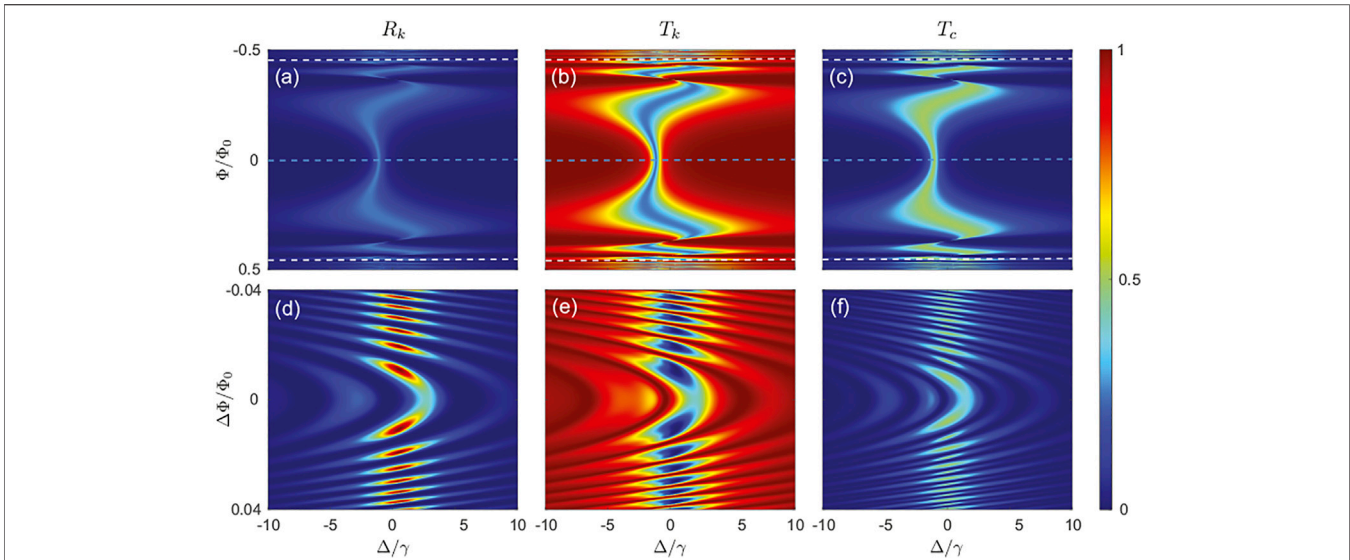


**FIGURE 3** | Density plots showing the single-photon **(A,D)** reflection rate  $R_k$ , **(B,E)** transmission rate  $T_k$ , and **(C,F)** frequency conversion rate  $T_c$  as a function of the detuning  $\Delta/\gamma$  and flux  $\Phi/\Phi_0$ . In **(A–C)**, the variation range of  $\Phi$  is set to be  $-0.5\Phi_0 \sim 0.5\Phi_0$  while **(D–F)** is  $-0.04\Phi_0 + \Phi_a \sim 0.04\Phi_0 + \Phi_a$  with  $\Phi_a$  satisfying  $\gamma T_a = \gamma T_0 / \sqrt{\cos(\pi\Phi_a/\Phi_0)} = 1$ .

significantly affected by the traveling time  $T$  with the maximum reflection rate increasing and the minimum transmission rate decreasing, respectively, as shown in **Figures 4A,B**. Apart from the main peak around the zero detuning, some small peaks arise on two sides of the resonance point. In contrast, the peaks of the frequency conversion rates for two cases only exhibit a slight shift, as shown in **Figure 4C**.

Based on the facts presented in **Figures 3, 4**, we find that the maximum reflection rate in the non-Markovian regime is much bigger than the corresponding rate in the Markovian regime with a narrower peak width. Giant atoms prefer to intensely interact with the photon modes with certain frequencies because these photon modes were selected out in a “cavity” formed by the two coupling points of the artificial giant atom, which acts as resonant mirrors [44].

Distinguishing scattering properties in both Markovian and non-Markovian regimes can serve future quantum technologies. Excitingly, all of these are now implemented by using one setup, in which we only need to change the external magnetic field through the SQUID loops. In addition, our circuit allows observing the transition between these two regimes by only modulating the external field gradually from one to the other.

## 4.2 Application: Quantum Storage

The tunable traveling time in our  $\Lambda$ -type giant atom can also be used to store quantum information. Because the corrected decay rates  $\Gamma_i$  depend on the phases, we can find an unusual phase  $\omega_c T$ , with which  $\Gamma_2$  can reach the maximum value as well as  $\Gamma_1$  at its minimum value. These tunable decay rates enable one to realize state transition between  $|b\rangle$  and  $|c\rangle$  in our system. For example,  $|b\rangle \rightarrow |a\rangle \rightarrow |c\rangle$  transitions can be achieved by switching off the decay  $\Gamma_1$ , when the atom is excited by an incident  $\omega_k$  photon.

Recalling **Eq. 7** with the initial values,  $C_a(0) = 1$ ,  $C_{bs}(0)$ , and  $C_{cs}(0) = 0$ , we obtain the atomic excitation

$$C_a(t) = \frac{1}{2\pi i} \int ds \frac{e^{st}}{s + i\omega_a + \gamma_1 D_1 + \gamma_2 D_2}. \quad (23)$$

The emission spectrum of outgoing photons in the long-time limit is

$$C_{bak}(\infty) = \frac{e^{-i\omega_k t} \sqrt{\gamma_1/\pi} \cos(\omega_k T/2)}{i(\omega_a - \omega_k) + \gamma_1(1 + e^{i\omega_k T}) + \gamma_2(1 + e^{i\omega_q T})}, \quad (24)$$

$$C_{caq}(\infty) = \frac{e^{-i\omega_q t} \sqrt{\gamma_2/\pi} \cos(\omega_q T/2)}{i(\omega_a - \omega_q) + \gamma_1(1 + e^{i\omega_k T}) + \gamma_2(1 + e^{i\omega_q T})}. \quad (25)$$

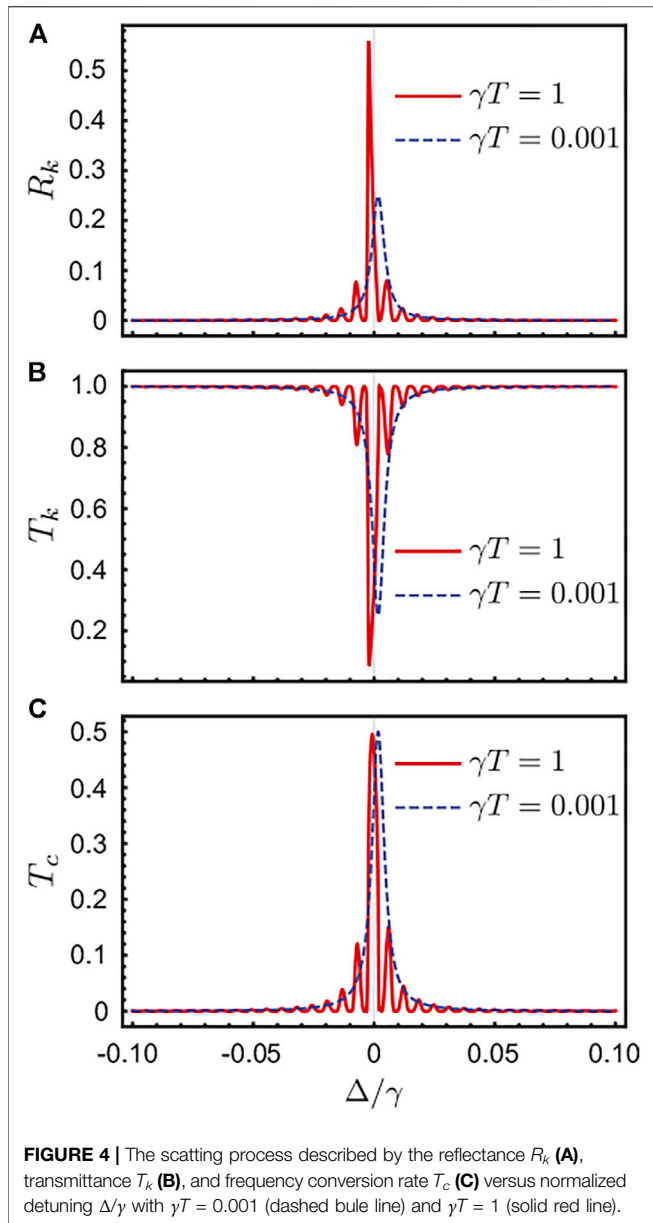
When the phases satisfy the conditions,  $\omega_k T_1 = \omega_{ab} T_1 = (2n + 1)\pi$  and  $\omega_q T_1 = \omega_{ac} T_1 = 2n\pi$ , the resonant photon with frequency  $\omega_{ab}$  [ $C_{bak}(\infty)$ ] vanishes corresponding to extreme depression of the decay path  $|a\rangle \rightarrow |b\rangle$ , while the conversion photon with frequency  $\omega_{ac}$  [ $C_{caq}(\infty)$ ] reaches the maximum corresponding to the enhancement of the decay from  $|a\rangle \rightarrow |c\rangle$ .

Using Residue theorem, we can derive  $C_a(t) = L^{-1}[C_a(s)] = \sum_n \text{Res}[C_a(s), s_n] e^{s_n t}$ , where  $s_n$  is the root of the equation [29,45].

$$s + i\omega_a + \gamma_1(1 + e^{-i\omega_b T} e^{-sT}) + \gamma_2(1 + e^{-i\omega_c T} e^{-sT}) = 0. \quad (26)$$

Interestingly, when  $s_n$  is a purely imaginary number  $s_n = i\omega_s$ , there will be a mode  $s_n$  without decay which can survive in the long time limit. Therefore, we have the stationary solution

$$C_a(t \rightarrow \infty) = \frac{e^{-i\omega_s t}}{1 - (\gamma_1 e^{-i\omega_b T} + \gamma_2 e^{-i\omega_c T}) T e^{-i\omega_s T}}, \quad (27)$$



which yields a dark state decoupled with the open transmission line.

If the giant atom is initially prepared in the excited state and the transition frequencies between levels satisfy  $\omega_{ac} = \omega_{ab} = (2n + 1)\pi/T$ , a dark-state mode,  $s_n = -i\omega_a$ ,  $C_a(t \rightarrow \infty) = \frac{e^{-i\omega_a t}}{1 + (\gamma_1 + \gamma_2)T}$ , exists. The fields in the transmission line have the form as

$$C_b(x, t) = \sqrt{\frac{\gamma_1}{2v_g}} (-1)^n e^{-i\omega_a t} 2 \cos\left(\frac{\omega_{ab}x}{v_g}\right) \times \Theta(-x + L/2)\Theta(x + L/2), \quad (28)$$

$$C_c(x, t) = \sqrt{\frac{\gamma_2}{2v_g}} (-1)^n e^{-i\omega_a t} 2 \cos\left(\frac{\omega_{ac}x}{v_g}\right) \times \Theta(-x + L/2)\Theta(x + L/2), \quad (29)$$

which are referring to continuum bound states [31,32]; [46,47]. Unlike the bound state protected by the energy gap [48-55], it derives from the destructive interference among the coupling points of the giant atom. Particularly, it can be created and relieved after introducing the adjustable traveling time. This method of preserving quantum information in an atom-waveguide bound state could be widely applied in quantum storage.

## 5 CONCLUSION

In this paper, we investigate a driven resonator-qubit giant  $\Lambda$ -type atom coupling to a SQUID-chain waveguide. By studying the scattering effect of individual photons on this giant atomic system, we explore both Markovian and non-Markovian phenomena caused by the interference effect between two coupling points. Due to the adjustable group velocity of the waveguide, the scattering effect of this artificial giant  $\Lambda$ -type atom to the incident microwave photon can show significant variation when we control the external magnetic field applied on SQUID loops in this particular waveguide. This in-situ modulation brings convenience to adjust the transmission of quantum information and provides more possibilities in future quantum technologies. Moreover, this setup can be realized in experiments using current state-of-the-art technologies for superconducting circuits [30]; [21,22]; [56].

## 6 APPENDIX

### 6.1 Derivation of the Giant Atom System

#### 6.1.1 Artificial $\Lambda$ -type Three-Level Atom

The artificial  $\Lambda$ -type giant atom can be realized in the design of the system of Ref. [36] in addition to one more coupling point in the waveguide-CPW resonator interface as shown in **Figure 1A**. The Hamiltonian of the qubit-resonator system is given by

$$H_s = \frac{\hbar}{2}\omega_q\sigma_z + \hbar\omega_r\left(a^\dagger a + \frac{1}{2}\right) + \hbar g\left(a^\dagger\sigma_- + a\sigma_+\right) + \hbar\left[\Omega\sigma_- \exp(i\omega_d t) + \Omega^*\sigma_+ \exp(-i\omega_d t)\right], \quad (30)$$

where  $\sigma_i$  are the pauli operators of the flux qubit with frequency  $\omega_q$ .  $a^\dagger(a)$  is the creation (annihilation) operator of the resonator  $\omega_r$  photon.  $g$  denotes the coupling constant of the qubit and the resonator, while  $\Omega$  is the Rabi frequency representing the amplitude of driving field  $E(t)$ . This system has a set of polarization states  $|1\rangle$ ,  $|2\rangle$ ,  $|3\rangle$ , and  $|4\rangle$ , which can be approximated as [37]:

$$\begin{aligned} |1\rangle &= -\sin\left(\frac{\theta_0}{2}\right)|\overline{e}, 0\rangle + \cos\left(\frac{\theta_0}{2}\right)|\overline{g}, 0\rangle, \\ |2\rangle &= \cos\left(\frac{\theta_0}{2}\right)|\overline{e}, 0\rangle + \sin\left(\frac{\theta_0}{2}\right)|\overline{g}, 0\rangle, \\ |3\rangle &= -\sin\left(\frac{\theta_1}{2}\right)|\overline{e}, 1\rangle + \cos\left(\frac{\theta_1}{2}\right)|\overline{g}, 1\rangle, \\ |4\rangle &= \cos\left(\frac{\theta_1}{2}\right)|\overline{e}, 1\rangle + \sin\left(\frac{\theta_1}{2}\right)|\overline{g}, 1\rangle, \end{aligned} \quad (31)$$

where the mixing angles  $\theta_0$  and  $\theta_1$  are given by  $\tan(\theta_0) = \Omega_d / [(\omega_q - \chi) - \omega_d]$  and  $\tan(\theta_1) = \Omega_d / [\omega_d - (\omega_q - 3\chi)]$ , respectively. And we use the set of polariton states  $|1\rangle, |2\rangle$  and  $|3\rangle$  to form a  $\Lambda$ -type system with the Hamiltonian  $H_s = \sum_j \tilde{\omega}_j |j\rangle \langle j| = \sum_j \tilde{\omega}_j \tilde{\sigma}_{jj}$ .

### 6.1.2 SQUID-Chain Waveguide

The SQUID-chain microwave transmission line model, as shown in **Figure 1**, can be described by the Hamiltonian

$$H_0 = \frac{1}{2} \vec{Q}^T \hat{C}^{-1} \vec{Q} + \vec{\Phi}^T \hat{L}^{-1} \vec{\Phi} = \sum_k \omega_k (a_k^\dagger a_k + 1/2), \quad (32)$$

where the charge and phase vectors have the form,  $\vec{Q}^T = (Q_1, Q_2, \dots, Q_N, \dots)$  and  $\vec{\Phi} = (\Phi_1, \Phi_2, \dots, \Phi_N, \dots)$ , respectively.  $\hat{C}$  and  $\hat{L}$  are the capacitance and inductance matrixes defined as [39]; [32].

$$\hat{C} = \begin{pmatrix} C_J & -C_J & 0 & \dots \\ -C_J & 2C_J + C_g & -C_J & 0 & \dots \\ 0 & -C_J & 2C_J + C_g & -C_J & 0 & \dots \\ \vdots & 0 & \ddots & \ddots & \ddots & \ddots \end{pmatrix}, \quad (33)$$

and

$$\hat{L}^{-1} = \begin{pmatrix} \frac{1}{L_J} & -\frac{1}{L_J} & 0 & \dots \\ -\frac{1}{L_J} & \frac{2}{L_J} & -\frac{1}{L_J} & 0 & \dots \\ 0 & -\frac{1}{L_J} & \frac{2}{L_J} & -\frac{1}{L_J} & 0 & \dots \\ \vdots & 0 & \ddots & \ddots & \ddots & \ddots \end{pmatrix}, \quad (34)$$

respectively. The charge-density operator at the antinode position  $Q$  can be approximately, in the linear limit  $C_J = 0$  [32], expressed as

$$Q = -iC_g \sum_k \sqrt{\frac{\hbar\omega_k}{C_t}} (a_k^\dagger e^{ikx} - a_k e^{-ikx}), \quad (35)$$

$C_t = NC_g$  is the total capacitance of SQUID chains.

### 6.1.3 Coupling Between SQUID-Chain Waveguides and Artificial $\Lambda$ -type Giant Atoms

The resonator-part Hamiltonian in the resonator-qubit system is written as

$$H_r = \hbar\omega_r \left( a^\dagger a + \frac{1}{2} \right) = \frac{Q_r^2}{2C} + \frac{\Phi_r^2}{2L}, \quad (36)$$

$Q_r$  and  $\Phi_r$  are the charge operator and the flux operator of the resonator, while  $C$  and  $L$  are the circuit characteristic capacitance and inductance, respectively. When a microwave field is incident, the Hamiltonian of the circuit resonator can be rewritten as

$$H_r = \frac{(Q_r + Q_e)^2}{2C} + \frac{\Phi_r^2}{2L}. \quad (37)$$

From **Eq. 35**, we know that the charge induced by the incident field is

$$Q_e(\pm x) = \frac{Q(\pm x)C_J^{g\pm}}{C_g} = -i \sum_k C_J^{g\pm} \sqrt{\frac{\hbar\omega_k}{C_t}} \times (a_k e^{ikx\pm} - a_k^\dagger e^{-ikx\pm}). \quad (38)$$

Expanding **Eq. 37** as

$$\begin{aligned} \frac{(Q_r + Q_e)^2}{2C} + \frac{\Phi_r^2}{2L} &= \frac{Q_r^2}{2C} + \frac{\Phi_r^2}{2L} + \frac{Q_r Q_e}{C} \\ &\approx \hbar\omega_r \left( a^\dagger a + \frac{1}{2} \right) + \hbar \sum_{\pm} \sum_k \frac{C_J^{g\pm}}{C} \sqrt{\frac{C}{C_t}} \sqrt{\frac{\omega_k \omega_r}{2}} (a_k^\dagger a e^{-ikx\pm} \\ &\quad + a_k a^\dagger e^{ikx\pm}), \end{aligned} \quad (39)$$

we obtain the radiative decay rate  $\kappa$  from the resonator to the waveguide,  $\sqrt{\kappa_{\pm}/2\pi} = C_J^{g\pm} \sqrt{C\omega_k \omega_r / 2C_t} / C_{\Sigma}$ .

Consequently, the total Hamiltonian of the system including the SQUID-chain waveguide and artificial  $\Lambda$ -type giant atom can be obtained as

$$\begin{aligned} H &= H_a + H_w + H_{int} \\ &= \sum_j \tilde{\omega}_j \tilde{\sigma}_{jj} + \int d\omega_k a_k^\dagger a_k \\ &\quad + \sum_{x_{\pm}} \int d\omega_k \sum_{i,j} \sqrt{\kappa_{ij}^{\pm}} / 2\pi (\tilde{\sigma}_{ij} a_k e^{ikx_{\pm}} + a_k^\dagger \tilde{\sigma}_{ji} e^{-ikx_{\pm}}), \end{aligned} \quad (40)$$

where  $\kappa_{ij}^{\pm} = \kappa | \langle i | a^\dagger | j \rangle |^2$  are equal to  $\gamma_i/2$  in the main text.

## 6.2 Derivation of the Single-Photon Process

In this part, we briefly derive the photon distribution and time evolution of the single-photon process. From the single-excitation wave function **Eq. 5**, we can substitute the state formula into the Schrödinger equation and obtain the dynamical equation for the giant atom

$$\begin{aligned} \frac{dC_a(t)}{dt} &= -i\omega_a C_a(t) \\ &\quad - i \sum_{a=1,2} \int \hbar \sqrt{\frac{\gamma_1}{4\pi}} C_{bak}(t) (e^{-i\omega_a \omega_k T/2} + e^{i\omega_a \omega_k T/2}) d\omega_k \\ &\quad - i \sum_{a=1,2} \int \hbar \sqrt{\frac{\gamma_2}{4\pi}} C_{caq}(t) (e^{-i\omega_a \omega_q T/2} + e^{i\omega_a \omega_q T/2}) d\omega_q. \end{aligned} \quad (41)$$

The propagating photon fields in the transmission line can be written as

$$\begin{aligned} \frac{dC_{bak}(t)}{dt} &= -i(\omega_b + \omega_k) C_{bak}(t) \\ &\quad - i \sqrt{\frac{\gamma_1}{4\pi}} C_a(t) (e^{-i\omega_a \omega_k T/2} + e^{i\omega_a \omega_k T/2}), \\ \frac{dC_{caq}(t)}{dt} &= -i(\omega_c + \omega_q) C_{caq}(t) \\ &\quad - i \sqrt{\frac{\gamma_2}{4\pi}} C_a(t) (e^{-i\omega_a \omega_q T/2} + e^{i\omega_a \omega_q T/2}). \end{aligned} \quad (42)$$

By integrating above equations, we can obtain **Eq. 6**. Then taking Laplace transform  $C_a(s) = \int_0^\infty C_a(t) e^{-st} dt$  and

introducing the coupling strength  $V_{1(2)} = \sqrt{\gamma_{1(2)}v_g/2}$ , the differential equation can be simplified to

$$\begin{aligned} sC_a(s) - C_a(0) &= -i\omega_a C_a(s) - D_1 C_a(s) - D_2 C_a(s) \\ -iV_1 \sqrt{\frac{2\pi}{v_g}} e^{-i\omega_b t} [C_{b1s}(0) + C_{b2s}(0)] (e^{sT/2} + e^{-sT/2}) \\ -iV_2 \sqrt{\frac{2\pi}{v_g}} e^{-i\omega_c t} [C_{c1s}(0) + C_{c2s}(0)] (e^{sT/2} + e^{-sT/2}). \end{aligned} \quad (43)$$

Here we set the right-propagating incident photon field  $C_{b1k}(0) \neq 0$ , which frequency band is around  $\omega_{ab}$ . With the giant atom initially being in the ground state, the probability amplitude of the excited state is given by

$$C_a(t) = -i\sqrt{\frac{\gamma_1}{4\pi}} \int ds \frac{C_{b1s}(0)(e^{sT/2} + e^{-sT/2})e^{st}e^{-i\omega_b t}}{s + i\omega_a + \gamma_1 D_1 + \gamma_2 D_2}. \quad (44)$$

From Eq. 42, we obtain the solutions of the forward-scattered field

$$\begin{aligned} C_{b1k}(t) &= e^{-i(\omega_b+\omega_k)t} \left[ C_{b1k}(0) - \frac{\gamma_1}{4\pi} (e^{-i\omega_k T/2} + e^{i\omega_k T/2}) \right. \\ &\quad \times \int ds \frac{C_{b1s}(0)(e^{sT/2} + e^{-sT/2})e^{st'}e^{-i\omega_b t'}}{s + i\omega_a + \gamma_1 D_1 + \gamma_2 D_2} \\ &\quad \left. \times \int_0^t dt' e^{i(\omega_b+\omega_k)t'} \right], \end{aligned} \quad (45)$$

$$\begin{aligned} C_{c1q}(t) &= e^{-i(\omega_c+\omega_q)t} \left[ -\sqrt{\frac{\gamma_1\gamma_2}{(4\pi)^2}} (e^{-i\omega_q T/2} + e^{i\omega_q T/2}) \right. \\ &\quad \times \int ds \frac{C_{b1s}(0)(e^{sT/2} + e^{-sT/2})e^{st'}e^{-i\omega_b t'}}{s + i\omega_a + \gamma_1 D_1 + \gamma_2 D_2} \\ &\quad \left. \times \int_0^t dt' e^{i(\omega_c+\omega_q)t'} \right], \end{aligned} \quad (46)$$

## REFERENCES

1. You JQ, Nori F. Atomic Physics and Quantum Optics Using Superconducting Circuits. *Nature* (2011) 474:589–97. doi:10.1038/nature10122
2. Xiang Z-L, Ashhab S, You JQ, Nori F. Hybrid Quantum Circuits: Superconducting Circuits Interacting with Other Quantum Systems. *Rev Mod Phys* (2013) 85:623–53. doi:10.1103/RevModPhys.85.623
3. Clarke J, Wilhelm FK. Superconducting Quantum Bits. *Nature* (2008) 453:1031–42. doi:10.1038/nature07128
4. Kimble HJ. The Quantum Internet. *Nature* (2008) 453:1023–30. doi:10.1038/nature07127
5. Ladd TD, Jelezko F, Laflamme R, Nakamura Y, Monroe C, O'Brien JL. Quantum Computers. *Nature* (2010) 464:45–53. doi:10.1038/nature08812
6. Blais A, Huang R-S, Wallraff A, Girvin SM, Schoelkopf RJ. Cavity Quantum Electrodynamics for Superconducting Electrical Circuits: An Architecture for Quantum Computation. *Phys Rev A* (2004) 69:062320. doi:10.1103/PhysRevA.69.062320
7. Wallraff A, Schuster DI, Blais A, Frunzio L, Huang RS, Majer J, et al. Strong Coupling of a Single Photon to a Superconducting Qubit Using Circuit Quantum Electrodynamics. *Nature* (2004) 431:162–7. doi:10.1038/nature02851
8. Johansson J, Saito S, Meno T, Nakano H, Ueda M, Semba K, et al. Vacuum Rabi Oscillations in a Macroscopic Superconducting Qubit/LCOscillator System. *Phys Rev Lett* (2006) 96:127006. doi:10.1103/PhysRevLett.96.127006

and the backward-scattered fields

$$\begin{aligned} C_{b2k}(t) &= e^{-i(\omega_b+\omega_k)t} \left[ -\frac{\gamma_1}{4\pi} (e^{-i\omega_k T/2} + e^{i\omega_k T/2}) \right. \\ &\quad \times \int ds \frac{C_{b1s}(0)(e^{sT/2} + e^{-sT/2})e^{st'}e^{-i\omega_b t'}}{s + i\omega_a + \gamma_1 D_1 + \gamma_2 D_2} \\ &\quad \left. \times \int_0^t dt' e^{i(\omega_b+\omega_k)t'} \right], \end{aligned} \quad (47)$$

where  $D_{1(2)} = 1 + e^{-i\omega_{b(c)}T} e^{-sT}$  is the phase of the decay rate sourced from the coupling points distance, defined in Sec.3.1 of the main text. After taking the long-time limit, we can finally solve the above integrations and obtain the scattering rates  $R_k$ ,  $T_k$  and  $T_q$  in Eqs. 12–14.

## DATA AVAILABILITY STATEMENT

The original contributions presented in the study are included in the article/Supplementary Material, further inquiries can be directed to the corresponding author.

## AUTHOR CONTRIBUTIONS

Z-LX initiated and supervised the project. J-PZ and Z-LX developed the theoretical model. J-PZ and R-YG performed the numerical plots. J-PZ and Z-LX wrote the draft. All authors contributed to the theoretical discussions, numerical plots analysis, and manuscript writing.

## FUNDING

The National Natural Science Foundation of China (Grant No. 11874432), and the National Key R&D Program of China (Grant No. 2019YFA0308200).

9. Astafiev O, Inomata K, Niskanen AO, Yamamoto T, Pashkin YA, Nakamura Y, et al. Single Artificial-Atom Lasing. *Nature* (2007) 449:588–90. doi:10.1038/nature06141
10. Abdumalikov AA, Astafiev O, Nakamura Y, Pashkin YA, Tsai J. Vacuum Rabi Splitting Due to strong Coupling of a Flux Qubit and a Coplanar-Waveguide Resonator. *Phys Rev B* (2008) 78:180502. doi:10.1103/PhysRevB.78.180502
11. Hofheinz M, Wang H, Ansmann M, Bialczak RC, Lucero E, Neeley M, et al. Synthesizing Arbitrary Quantum States in a Superconducting Resonator. *Nature* (2009) 459:546–9. doi:10.1038/nature08005
12. Niemczyk T, Deppe F, Huebl H, Menzel EP, Hocke F, Schwarz MJ, et al. Circuit Quantum Electrodynamics in the Ultrastrong-Coupling Regime. *Nat Phys* (2010) 6:772–6. doi:10.1038/nphys1730
13. Astafiev O, Zagoskin AM, Abdumalikov AA, Pashkin YA, Yamamoto T, Inomata K, et al. Resonance Fluorescence of a Single Artificial Atom. *Science* (2010) 327:840–3. doi:10.1126/science.1181918
14. Paik H, Schuster DI, Bishop LS, Kirchmair G, Catelani G, Sears AP, et al. Observation of High Coherence in Josephson Junction Qubits Measured in a Three-Dimensional Circuit QED Architecture. *Phys Rev Lett* (2011) 107:240501. doi:10.1103/PhysRevLett.107.240501
15. Blais A, Grimsmo AL, Girvin SM, Wallraff A. Circuit Quantum Electrodynamics. *Rev Mod Phys* (2021) 93:025005. doi:10.1103/RevModPhys.93.025005
16. Koch J, Yu TM, Gambetta J, Houck AA, Schuster DI, Majer J, et al. Charge-insensitive Qubit Design Derived from the Cooper Pair Box. *Phys Rev A* (2007) 76:042319. doi:10.1103/PhysRevA.76.042319

17. Barends R, Kelly J, Megrant A, Sank D, Jeffrey E, Chen Y, et al. Coherent Josephson Qubit Suitable for Scalable Quantum Integrated Circuits. *Phys Rev Lett* (2013) 111:080502. doi:10.1103/PhysRevLett.111.080502
18. Frisk Kockum A. Quantum Optics with Giant Atoms—The First Five Years. In: T Takagi, M Wakayama, K Tanaka, N Kunihiro, K Kimoto, Y Ikematsu, editors. *International Symposium on Mathematics, Quantum Theory, and Cryptography*. Singapore: Springer Singapore (2021). p. 125–46. doi:10.1007/978-981-15-5191-8\_12
19. Gustafsson MV, Aref T, Kockum AF, Ekström MK, Johansson G, Delsing P. Propagating Phonons Coupled to an Artificial Atom. *Science* (2014) 346:207–11. doi:10.1126/science.1257219
20. Manenti R, Kockum AF, Patterson A, Behrle T, Rahamim J, Tancredi G, et al. Circuit Quantum Acoustodynamics with Surface Acoustic Waves. *Nat Commun* (2017) 8:975. doi:10.1038/s41467-017-01063-9
21. Guimond P-O, Vermersch B, Juan ML, Sharafiev A, Kirchmair G, Zoller P. A Unidirectional On-Chip Photonic Interface for Superconducting Circuits. *Npj Quan Inf* (2020) 6:32. doi:10.1038/s41534-020-0261-9
22. Kannan B, Ruckriegel MJ, Campbell DL, Frisk Kockum A, Braumüller J, Kim DK, et al. Waveguide Quantum Electrodynamics with Superconducting Artificial Giant Atoms. *Nature* (2020) 583:775–9. doi:10.1038/s41586-020-2529-9
23. Frisk Kockum A, Delsing P, Johansson G. Designing Frequency-dependent Relaxation Rates and Lamb Shifts for a Giant Artificial Atom. *Phys Rev A* (2014) 90:013837. doi:10.1103/PhysRevA.90.013837
24. Zhao W, Wang Z. Single-photon Scattering and Bound States in an Atom-Waveguide System with Two or Multiple Coupling Points. *Phys Rev A* (2020) 101:053855. doi:10.1103/PhysRevA.101.053855
25. Yu H, Wang Z, Wu J-H. Entanglement Preparation and Nonreciprocal Excitation Evolution in Giant Atoms by Controllable Dissipation and Coupling. *Phys Rev A* (2021) 104:013720. doi:10.1103/PhysRevA.104.013720
26. Yin X-L, Liu Y-H, Huang J-F, Liao J-Q. Single-photon Scattering in a Giant-Molecule Waveguide-Qed System. *arXiv:2203.07812v1* (2022). doi:10.48550/ARXIV.2203.07812
27. Andersson G, Ekström MK, Delsing P. Electromagnetically Induced Acoustic Transparency with a Superconducting Circuit. *Phys Rev Lett* (2020) 124:240402. doi:10.1103/PhysRevLett.124.240402
28. de Vega I, Alonso D. Dynamics of Non-markovian Open Quantum Systems. *Rev Mod Phys* (2017) 89:1. doi:10.1103/RevModPhys.89.015001
29. Guo L, Grimsmo A, Kockum AF, Pletyukhov M, Johansson G. Giant Acoustic Atom: A Single Quantum System with a Deterministic Time Delay. *Phys Rev A* (2017) 95:053821. doi:10.1103/PhysRevA.95.053821
30. Andersson G, Suri B, Guo L, Aref T, Delsing P. Non-exponential Decay of a Giant Artificial Atom. *Nat Phys* (2019) 15:1123–7. doi:10.1038/s41567-019-0605-6
31. Guo L, Kockum AF, Marquardt F, Johansson G. Oscillating Bound States for a Giant Atom. *Phys Rev Res* (2020) 2:043014. doi:10.1103/PhysRevResearch.2.043014
32. Wang X, Liu T, Kockum AF, Li H-R, Nori F. Tunable Chiral Bound States with Giant Atoms. *Phys Rev Lett* (2021) 126:043602. doi:10.1103/PhysRevLett.126.043602
33. Sheremet AS, Petrov MI, Iorsh IV, Poshakinskiy AV, Poddubny AN. Waveguide Quantum Electrodynamics: Collective Radiances and Photon-Photon Correlations. *arXiv e-prints, arXiv:2103.06824* (2021).
34. Kockum AF, Johansson G, Nori F. Decoherence-free Interaction between Giant Atoms in Waveguide Quantum Electrodynamics. *Phys Rev Lett* (2018) 120:140404. doi:10.1103/PhysRevLett.120.140404
35. Du L, Li Y. Single-photon Frequency Conversion via a Giant  $\Lambda$ -type Atom. *Phys Rev A* (2021) 104:023712. doi:10.1103/PhysRevA.104.023712
36. Inomata K, Koshino K, Lin ZR, Oliver WD, Tsai JS, Nakamura Y, et al. Microwave Down-Conversion with an Impedance-Matched System in Driven Circuit QED. *Phys Rev Lett* (2014) 113:063604. doi:10.1103/PhysRevLett.113.063604
37. Long J, Ku HS, Wu X, Gu X, Lake RE, Bal M, et al. Electromagnetically Induced Transparency in Circuit Quantum Electrodynamics with Nested Polariton States. *Phys Rev Lett* (2018) 120:083602. doi:10.1103/PhysRevLett.120.083602
38. Rakhmanov AL, Zagoskin AM, Savel'ev S, Nori F. Quantum Metamaterials: Electromagnetic Waves in a Josephson Qubit Line. *Phys Rev B* (2008) 77:144507. doi:10.1103/PhysRevB.77.144507
39. Weißl T, Küng B, Dumur E, Feofanov AK, Matei I, Naud C, et al. Kerr Coefficients of Plasma Resonances in Josephson Junction Chains. *Phys Rev B* (2015) 92:104508. doi:10.1103/PhysRevB.92.104508
40. Krupko Y, Nguyen VD, Weißl T, Dumur E, Puertas J, Dassonneville R, et al. Kerr Nonlinearity in a Superconducting Josephson Metamaterial. *Phys Rev B* (2018) 98:094516. doi:10.1103/PhysRevB.98.094516
41. Puertas Martínez J, Léger S, Gheeraert N, Dassonneville R, Planat L, Foroughi F, et al. A Tunable Josephson Platform to Explore many-body Quantum Optics in Circuit-Qed. *Npj Quan Inf* (2019) 5:19. doi:10.1038/s41534-018-0104-0
42. Planat L, Ranadive A, Dassonneville R, Puertas Martínez J, Léger S, Naud C, et al. Photonic-crystal Josephson Traveling-Wave Parametric Amplifier. *Phys Rev X* (2020) 10:021021. doi:10.1103/PhysRevX.10.021021
43. Shen JT, Fan S. Coherent Photon Transport from Spontaneous Emission in One-Dimensional Waveguides. *Opt Lett* (2005) 30:2001–3. doi:10.1364/OL.30.002001
44. Mirhosseini M, Kim E, Zhang X, Sipahigil A, Dieterle PB, Keller AJ, et al. Cavity Quantum Electrodynamics with Atom-like Mirrors. *Nature* (2019) 569:692–7. doi:10.1038/s41586-019-1196-1
45. Guo S, Wang Y, Purdy T, Taylor J. Beyond Spontaneous Emission: Giant Atom Bounded in the Continuum. *Phys Rev A* (2020) 102:033706. doi:10.1103/PhysRevA.102.033706
46. Hsu CW, Zhen B, Stone AD, Joannopoulos JD, Soljačić M. Bound States in the Continuum. *Nat Rev Mater* (2016) 1:16048. doi:10.1038/natrevmats.2016.48
47. Calajó G, Fang Y-LL, Baranger HU, Ciccarello F. Exciting a Bound State in the Continuum through Multiphoton Scattering Plus Delayed Quantum Feedback. *Phys Rev Lett* (2019) 122:073601. doi:10.1103/PhysRevLett.122.073601
48. Longo P, Schmitteckert P, Busch K. Few-photon Transport in Low-Dimensional Systems: Interaction-Induced Radiation Trapping. *Phys Rev Lett* (2010) 104:023602. doi:10.1103/PhysRevLett.104.023602
49. Shahmoon E, Kurizki G. Nonradiative Interaction and Entanglement between Distant Atoms. *Phys Rev A* (2013) 87:033831. doi:10.1103/PhysRevA.87.033831
50. Calajó G, Ciccarello F, Chang D, Rabl P. Atom-field Dressed States in Slow-Light Waveguide Qed. *Phys Rev A* (2016) 93:033833. doi:10.1103/PhysRevA.93.033833
51. Liu Y, Houck AA. Quantum Electrodynamics Near a Photonic Bandgap. *Nat Phys* (2017) 13:48–52. doi:10.1038/nphys3834
52. González-Tudela A, Cirac JI. Markovian and Non-markovian Dynamics of Quantum Emitters Coupled to Two-Dimensional Structured Reservoirs. *Phys Rev A* (2017) 96:043811. doi:10.1103/PhysRevA.96.043811
53. González-Tudela A, Cirac JI. Quantum Emitters in Two-Dimensional Structured Reservoirs in the Nonperturbative Regime. *Phys Rev Lett* (2017) 119:143602. doi:10.1103/PhysRevLett.119.143602
54. Sundaresan NM, Lundgren R, Zhu G, Gorshkov AV, Houck AA. Interacting Qubit-Photon Bound States with Superconducting Circuits. *Phys Rev X* (2019) 9:011021. doi:10.1103/PhysRevX.9.011021
55. Leonforte L, Carollo A, Ciccarello F. Vacancy-like Dressed States in Topological Waveguide Qed. *Phys Rev Lett* (2021) 126:063601. doi:10.1103/PhysRevLett.126.063601
56. Vadiraj AM, Ask A, McConkey TG, Nsanzineza I, Chang CWS, Kockum AF, et al. Engineering the Level Structure of a Giant Artificial Atom in Waveguide Quantum Electrodynamics. *Phys Rev A* (2021) 103:023710. doi:10.1103/PhysRevA.103.023710

**Conflict of Interest:** The authors declare that the research was conducted in the absence of any commercial or financial relationships that could be construed as a potential conflict of interest.

**Publisher's Note:** All claims expressed in this article are solely those of the authors and do not necessarily represent those of their affiliated organizations, or those of the publisher, the editors and the reviewers. Any product that may be evaluated in this article, or claim that may be made by its manufacturer, is not guaranteed or endorsed by the publisher.

Copyright © 2022 Zou, Gong and Xiang. This is an open-access article distributed under the terms of the Creative Commons Attribution License (CC BY). The use, distribution or reproduction in other forums is permitted, provided the original author(s) and the copyright owner(s) are credited and that the original publication in this journal is cited, in accordance with accepted academic practice. No use, distribution or reproduction is permitted which does not comply with these terms.